

Stray field signatures of Néel textured skyrmions in Ir/Fe/Co/Pt multilayer films

A. Yagil,¹ A. Almoalem,¹ Anjan Soumyanarayanan,^{2,3} Anthony K. C. Tan,^{2,3} M. Raju,² C. Panagopoulos,^{2,*} and O. M. Auslaender^{1,†}

¹*Department of Physics, Technion, Haifa 32000, Israel*

²*Division of Physics and Applied Physics, School of Physical and Mathematical Sciences, Nanyang Technological University, 637371 Singapore*

³*Data Storage Institute, 2 Fusionopolis Way, 138634 Singapore*

The development of technologically relevant skyrmions in multilayer films requires magnetic imaging methods sensitive to their spin structure, yet translatable to device configurations. We present a multipole expansion to quantitatively describe the magnetic field of individual skyrmions in magnetic force microscopy. By using specific multipole signatures of skyrmions of different spin structure, we establish their Néel texture and helicity in a Ir/Fe/Co/Pt film. The demonstrated sensitivity to inhomogeneity provides a route for characterizing individual skyrmions in devices.

The realization of magnetic skyrmions in metallic multilayer films has generated a surge of research [1–4]. Skyrmions are chiral magnetic structures which can remain stable despite their small size. Their unique properties stem from their topologically non-trivial spin texture. Understanding the structure and behavior of these localized two-dimensional (2D) objects is of fundamental scientific importance [5–7], with implications for next-generation memory technologies [6, 8, 9]. The spin at the center of a skyrmion is oriented opposite to the background out-of-plane (OP) magnetization [Fig. 2(a-d)]. The OP spin orientation aligns with the background over a length scale defining the skyrmion size (d_{Sk}), which can vary from a few nanometers to micron scale [10, 11]. Meanwhile, the in-plane (IP) spin component winds chirally, defining the skyrmion topology with a specific helicity (γ) [5], ranging from Néel [7] ($\gamma = 0, \pi$) to Bloch [12] ($\gamma = \pm\pi/2$) texture.

Skyrmions are formed due to the anti-symmetric Dzyaloshinskii-Moriya interaction (DMI) found in chiral magnets [12–16] and at ferromagnet/heavy-metal interfaces [17, 18]. Initial efforts to realize interfacial DMI were using epitaxial monolayers at low temperatures [1]. However, the focus has rapidly shifted to sputtered multilayer films – shown to host columnar room temperature (RT) skyrmions [2–4, 19, 20] stabilized by interlayer exchange coupling. The properties of these multilayer skyrmions show significantly more variation than their epitaxial counterparts. First, d_{Sk} can be inhomogeneous in sputtered films – with up to $\times 2$ variations over a micron range [3]. Next, the spin structure can vary [10] – with columnar skyrmions potentially consisting of inertial ‘cores’ [3, 4, 21]. Finally, the granularity of magnetic interactions can induce skyrmion pinning, resulting in variations in skyrmion configuration [20], directly affecting motion and switching [22]. It is therefore crucial to map and characterize individual skyrmions.

Real space imaging techniques, such as spin-polarized scanning tunneling microscopy (SP-STM) [1, 10, 23], X-ray magnetic circular dichroism (XMCD) [2–4], Lorentz

transmission electron microscopy (L-TEM) [24], nitrogen vacancy magnetometry (NVM) [25], and Kerr microscopy [11], have been instrumental in the detection and characterization of skyrmions in films [26], but have limited utility for investigating sub-100 nm skyrmions in realistic device configurations – due to customized sample preparation requirements or resolution limitations. In contrast, magnetic force microscopy (MFM) is a workhorse technique for determining magnetic properties of thin films down to the nanoscale with potential for device-directed efforts [22, 27]. However, in the absence of a simple physical model, the utility of MFM for quantitatively studying individual skyrmions [20] and investigating their topological properties remains questioned [27, 28] and is challenging to implement [29].

Here we demonstrate a magnetic-field-based method for quantitative studies of individual skyrmions in sputtered multilayer films hosting interfacial DMI. We harness signatures of a magnetic multipole expansion of the field from skyrmions (MEFS) for skyrmions with different spin structure, which can be captured quantitatively by MFM. MEFS allows us to go beyond the standard practice of characterizing the signal from a skyrmion by a Gaussian [3, 20], which is not justified by the microscopics. We thus establish the presence of Néel texture in our skyrmions, their size, and the sensitivity of these properties to inhomogeneity. MEFS is extendible to other field-sensitive microscopy techniques, and is easy to apply to large arrays of skyrmions. The results establish a means for quantitative characterization of individual skyrmions in device configurations.

In this work we study a multilayer film of [Ir(1)/Fe(0.5)/Co(0.5)/Pt(1)]₂₀ sputtered on SiO₂ substrates (total thickness, $d = 75$ nm) [30]. Ir/Fe/Co/Pt multilayers have previously been shown to host interfacial DMI, leading to the formation of sub-100 nm columnar skyrmions at RT [20]. The MFM results reported here were obtained at $T = 5$ K, and skyrmions were stabilized by sweeping up the magnetic field after saturating the magnetization at -0.5 T.

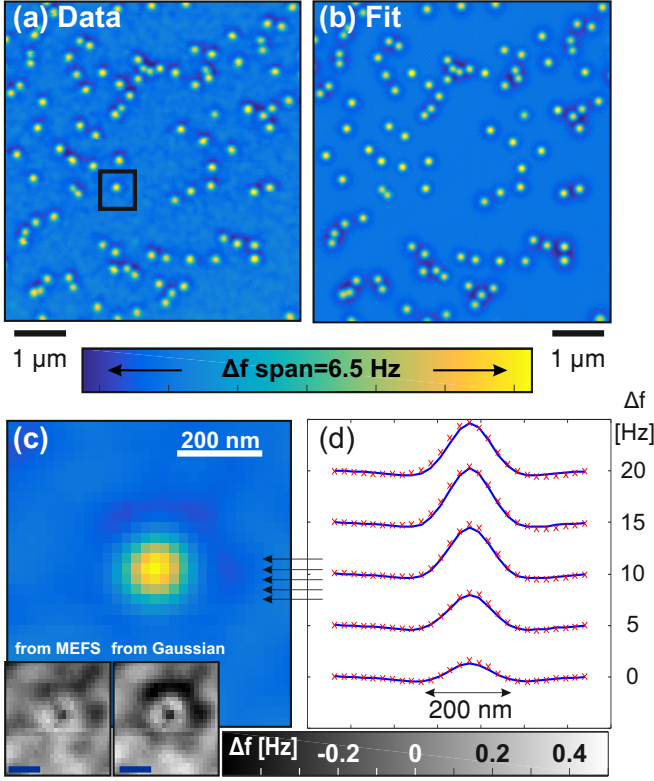


FIG. 1. (a) MFM image for $\mu_0 H = -0.3$ T with $h = 50$ nm. Black frame shows zoom area for (c). (b) Result of the MEFS fit. (c) Zoom on an individual skyrmion from (a). Arrows indicate the positions of line cuts in (d). **Insets:** the difference between the data and – the MEFS fit (left), and a 2D Gaussian fit (right). [Scale bars: 200 nm.] (d) Line cuts through the data (x's) in (c), offset for clarity, and the fit (lines).

MFM imaging is performed by rastering a sharp magnetic tip at a distance h from the planar ($x-y$) surface of the sample, with the tip-sample interaction force (F_z) giving the signal. Our system is frequency modulated [31] – we measure the F_z -induced changes of the resonant frequency (Δf) of the cantilever holding the tip. Such a response can be well-described provided that the cantilever motion is harmonic and that $\Delta f \ll f_0$, the natural resonant frequency [32]. Adapting to MFM raster scanning [30], the 2D Fourier transform (FT) of Δf is related to the FT of $\partial F_z / \partial h$, by $\widehat{\Delta f}_{\mathbf{k}}(h) = \mathcal{T}(ka) \widehat{\partial F_z / \partial h}$, where $k = (k_x^2 + k_y^2)^{1/2}$ and $\mathcal{T}(ka) = -k_0^{-1} f_0 I_1(ka) \exp(-ka) / (ka)$. Here k_0 is the spring constant of the cantilever and $I_1(x)$ is a Bessel function. Note that for $a \rightarrow 0$, $\mathcal{T}(ka) \approx -f_0 / 2k_0$, as expected [31]. For our MFM tips $f_0 \approx 75$ kHz, $k_0 \approx 1$ N/m and we used $a \approx 30$ nm, and set $h \lesssim 50$ nm for sufficiently high resolution.

Figure 1(a) is a typical MFM image acquired at $\mu_0 H = -0.3$ T, showing small round features – identified as skyrmions [20] – against a near-uniform background. Given that both the tip and sample were polarized at -0.5 T, the uniformly magnetized background interacts

weakly with the tip, with small variations indicating disorder [29]. In contrast, the skyrmions, magnetized opposite to the background, display a much stronger and repulsive interaction with the tip. Notably, the skyrmions are randomly dispersed suggesting that disorder is more important than skyrmion-skyrmion interactions at this density. Close inspection of Fig. 1(a) reveals that the skyrmions are not identical. We now focus on the shape of the signal from individual skyrmions [cf. Fig. 1(c)]. The standard practice is to fit this signal to a peak shape, e.g. a 2D Gaussian [cf. Fig. 1(c), right inset]. Here we provide an alternative framework for describing the MFM signal of skyrmions with improved accuracy [Fig. 1(c), left inset], which importantly has physical justification from a microscopic model.

An important requirement for the quantitative analysis of Fig. 1(a) is an accurate physical description of the signal from a skyrmion. We have found that the sum of a dipolar field and a quadrupolar field describes the magnetic field of a skyrmion well. Below we describe the motivation for this description, and examine the relationship between the dipole (P_i) and quadrupole (Q_{ij}) moments and the MFM signal.

In order to quantitatively reproduce the MFM signal, we need to model the magnetic field generated by a skyrmion. The local magnetization configuration of a skyrmion (\mathbf{M}) is defined by the magnetic interactions – interfacial DMI strength (D), exchange stiffness (A), and effective anisotropy (K), which also accounts for the demagnetization field. For a uniformly magnetized thin film hosting an axially-symmetric skyrmion with vorticity m magnetized along $\pm \hat{z}$, the local magnetization is [5]: $\mathbf{M}(\rho, z) / M_s(z) = \sin \theta(\rho) \cos \psi(\varphi) \hat{x} + \sin \theta(\rho) \sin \psi(\varphi) \hat{y} + [\pm 1 + \cos \theta(\rho)] \hat{z}$. Here $\psi(\varphi) = m\varphi + \gamma$ where φ is the axial angle, θ is the polar angle, $\rho = 2\pi r / L_D$ (r is the distance from the center of the skyrmion, $L_D \equiv 4\pi A / |D|$), $M_s(z) = M_s^0 [\Theta(z + d/2) - \Theta(z - d/2)]$, where M_s^0 is the saturation magnetization, and $\Theta(z)$ is the Heaviside function. $\theta(\rho)$ is a solution of well known ordinary differential equations [33]. In particular, for $\theta(0) = \pi$, $\theta(\infty) = 0$, and $m = 1$ for the relevant skyrmions [5, 6]:

$$\theta'' + \frac{\theta' + 2 \sin^2 \theta}{\rho} - \sin \theta \cos \theta (\rho^{-2} + k) - b \sin \theta = 0. \quad (1)$$

Here $k = K / K_0$ ($K_0 \equiv D^2 / 4A$ is the critical anisotropy) and $b = B / B_D$ ($B_D \equiv D^2 / 2AM_s^0$). A solution for typical parameters [34] is shown in Fig. 2(e).

The magnetic field from a localized magnetic structure, such as a skyrmion, can be described by a multipole expansion [35]. For this we define a magnetic scalar potential $\mathbf{H} = -\nabla \Phi$. Viewing $-\nabla \cdot \mathbf{M}$ as a magnetic analog of a charge distribution allows us to determine Φ , and consequently the MFM response [30]. The first term of the resulting MEFS (dipole) is proportional to $P_i \equiv -\int r_i \nabla \cdot \mathbf{M} dv$, and the second (quadrupole) to

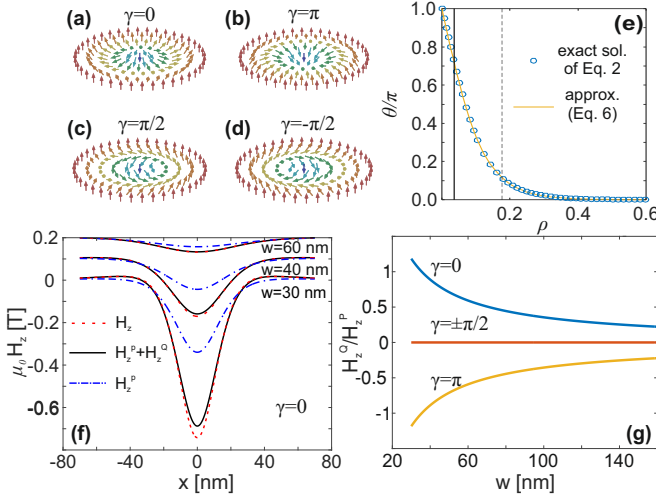


FIG. 2. (a-d) Schematic of the spins in Néel (a,b) and Bloch (c,d) skyrmions with $m = 1$ and $\gamma = 0, \pi, \pm\pi/2$. (e) Plot of $\theta(\rho)$ for $k = 1.536$, $b = 1.474$ [34] from a numerical solution of Eq. 1 (circles), and a fit to Eq. 5 (line), which gives: $\sigma = 0.140$, $\rho_0 = 0.037$. The vertical lines show ρ_0 (solid) and $\rho_0 + \sigma$ (dashed). $\rho = 2\pi d_{\text{Sk}}/L_D$ corresponds to $\theta/\pi = 0.5$. (f) The vertical field component, $\mu_0 H_z$, in a cut through the center of a skyrmion in a $d = 20$ nm thick film for various values of $w = h + d/2$, with the curves offset for clarity. Shown are $\mu_0 H_z$ obtained from $\theta(\rho)$ in (e) as well as from the dipole and quadrupole fields ($\equiv H_z^P$, $\equiv H_z^Q$) from Eqs. 3, 4 with $\gamma = 0$. (g) H_z^Q/H_z^P calculated using Eqs. 3, 4 for $\gamma = 0, \pm\pi/2, \pi$ as a function of w for $R = 0$.

$Q_{ij} \equiv -\int (3r_i r_j - \mathbf{r}^2 \delta_{ij}) \nabla \cdot \mathbf{M} dv$. For axially symmetric skyrmions with $m = 1$, we find $\mathbf{P} = P\hat{z}$ and a diagonal Q_{ij} , i.e. $Q_{xx} = Q_{yy} = -Q_{zz}/2 \equiv Q$. Thus:

$$\Phi(R, h) \approx \frac{1}{4\pi} \left(\frac{Pw}{(R^2 + w^2)^{3/2}} + \frac{Q}{2} \frac{R^2 - 2w^2}{(R^2 + w^2)^{5/2}} \right), \quad (2)$$

where $w = h + d/2$ and [30]:

$$P = 2\pi M_s^0 d \left(\frac{L_D}{2\pi} \right)^2 \int_0^\infty d\rho \rho \{ \pm 1 + \cos[\theta(\rho)] \}, \quad (3)$$

$$Q = 2\pi M_s^0 d \left(\frac{L_D}{2\pi} \right)^3 \cos \gamma \int_0^\infty d\rho \rho^2 \sin[\theta(\rho)]. \quad (4)$$

The sign of P gives the OP magnetization at the center of the skyrmion ($\pm\hat{z}$). Notably, the sign of Q indicates whether the IP magnetization points outward (+) or inward (−) with respect to the skyrmion center. Importantly for Bloch skyrmions $Q = 0$. For Néel skyrmions the sign of Q gives the helicity, which is difficult to extract from other imaging techniques [24].

To estimate P and Q , we approximate the solution of Eq. 1 [10]:

$$\pi - \theta(\rho) \approx \sin^{-1} [\tanh(\eta_+)] + \sin^{-1} [\tanh(\eta_-)], \quad (5)$$

where $\eta_{\pm} \equiv (\rho \pm \rho_0)/\sigma$, σ parameterizes the thickness of the skyrmion domain wall and ρ_0 parameterizes its

radius. For $\rho_0/\sigma \ll 1$ we obtain $Q/|P| \approx d_{\text{Sk}} \cos \gamma$, where $M_z(r = d_{\text{Sk}}) = 0$ [30]. For Fig. 2(e) a fit to Eq. 5 gives $\sigma = 0.140$ and $\rho_0 = 0.037 \ll \sigma$.

To substantiate our assertions we have performed rudimentary numerics for a film with $d = 20$ nm. Starting from the solution of Eq. 1 [cf. Fig. 2(e)] we calculate the magnetic field from the integral solution of the Poisson equation for Φ , and P and Q using Eqs. 3, 4. A comparison between the exact solution and the multipole expansion is presented in Fig. 2(f). Equation 2 describes the stray field very well. As expected, at large w the quadrupole contribution is small and becomes larger as w is reduced. Figure 2(g) shows the ratio between the quadrupole (H_z^Q) and the dipole (H_z^P) contributions to H_z , from Eqs. 2-4 with $\gamma = 0, \pm\pi/2, \pi$. As expected, for Bloch skyrmions ($\gamma = \pm\pi/2$) $Q = 0$, and the sign of Q is opposite for the two kinds of Néel skyrmions ($\gamma = 0, \pi$). Thus Q/P allows the direct determination of skyrmion helicity.

To fit the MFM data using Eq. 2, we need to account for the tip geometry. A scanning electron microscopy (SEM) image of our tip can be modeled as a thin shell with axial symmetry [30]: $M_z^t(\mathbf{R}, z) = m_0 \delta[|\mathbf{R}| - g(z)]$. Here $m_0 = M_0 t$, where M_0 is the tip magnetization and t is the thickness of the magnetic coating; z is along the tip axis and $g(z)$ is the height-dependent radius for constant z . Given $g(z)$, Eq. 2 implies:

$$\frac{\partial F_z}{\partial h} = -\frac{C}{2} \int_0^\infty dk \int_0^\infty dz k^4 \Phi_k J_0[g(z)k] g(z) J_0(Rk) e^{-k[w+z]}, \quad (6)$$

where Φ_k is the Fourier transform of $\Phi(R, h = 0)$, $J_0(x)$ is a Bessel function and C is a constant. A fit using Eq. 6 is computationally expensive. We therefore first determine the skyrmion positions by fitting to a simplified model of the tip [30]. The fit to this model describes the data well. We therefore also use it to characterize the data by calculating the full width at half maximum (FWHM) and the skyrmion peak height (Δf_{max}).

Having determined the skyrmion positions, we fit their profile, now using a more accurate tip model: $g(z) = \alpha(z^4 + \beta z)^{1/4}$, with $\alpha = 0.24$ and $\beta = 2.7 \times 10^6 \text{ nm}^3$ [30]. For the fit we set a value for w and then find the optimal values for C and Q/P that minimize the fit error χ^2 in a 700 nm square centered around each skyrmion. Figure 3(a) shows a typical example for the dependence of χ^2 on Q/P (using the optimal value for C) for a representative skyrmion using different values of w . Notably, regardless of w the $\chi^2(Q/P)$ curves show a local maximum at $Q/P = 0$. On the other hand the location of a shallow minimum depends on w . Above the upper bound for w (90 nm) the minimum is at $Q/P \lesssim 0$. Below the upper bound this global minimum switches to $Q/P \gtrsim 0$. We therefore conclude that $Q/P \gtrsim 0$ for the skyrmions in our film.

This individual fit procedure was repeated for all

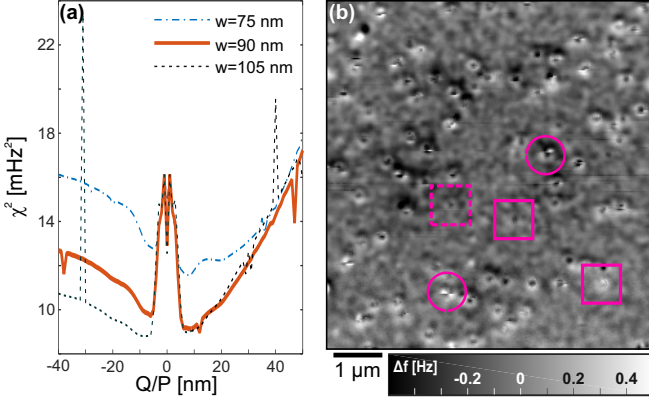


FIG. 3. (a) Plot of χ^2 for a representative skyrmion vs. Q/P for $w = 75, 90, 105$ nm. For each value of Q/P we chose a value of C that minimizes χ^2 in the area marked by the dashed rectangle in (b). (b) The difference between the data in Fig. 1(a) and the model where we fit each skyrmion individually. The dashed red rectangle shows a 700 nm square, where χ^2 is calculated for a representative skyrmion [in (a)]. We highlight the location of a few skyrmions that leave discontinuous residue (circles), and a few skyrmions that leave negligible residue (rectangles).

skyrmions using $w = 90 \text{ nm}$, and the residual difference between the data [Fig. 1(a)] and the fit [Fig. 1(b)] is shown in Fig. 3(b). Close inspection of Fig. 3(b) reveals several subtle features. First, the nanoscale variations observed in the background are typical of the inhomogeneous magnetic structure of sputtered magnetic multilayer films [29]. Second, discontinuities are observed at some skyrmion positions [e.g. circles in Fig. 3(b)], likely due to MFM tip-induced skyrmion motion (cf. superconducting vortices [38, 39]). Other explanations, such as irregular skyrmion shapes, cannot give sharp featured fit residuals. These observations, in conjunction with the structure of the background and the variability in skyrmion properties, are a direct consequence of inhomogeneous magnetic interactions [29], reinforcing the description of multilayer skyrmions using individual fit parameters.

Figure 4 shows histograms of the fit parameters from 98 skyrmions out of the 104 in Fig. 1(a). Panels (a,b) show the FWHM and Δf_{max} [30]. We show the parameters of the full fit in panels (c,d). First, we note that the FWHM (which includes tip effects) varies by $\sim 20\%$ ($100 - 120 \text{ nm}$), but is larger than RT values reported on similar films [20]. This difference can be ascribed to the change in magnetic parameters at 5 K . Notably however, the relative uniformity in FWHM [Fig. 4(a)] is in stark contrast to the variability in Δf_{max} [Fig. 4(b)].

Figure 4(c) shows two histograms – narrow and wide. The former is for the actual fit results for Q/P , but as the plot of C vs. Q/P and Fig. 3(a) show, the fit uncertainty is large. We therefore generated the wider histogram by assuming that each value of Q/P is drawn from a normal distribution $\mathcal{N}(Q/P, \delta Q/P)$ with the width $\delta Q/P$ given

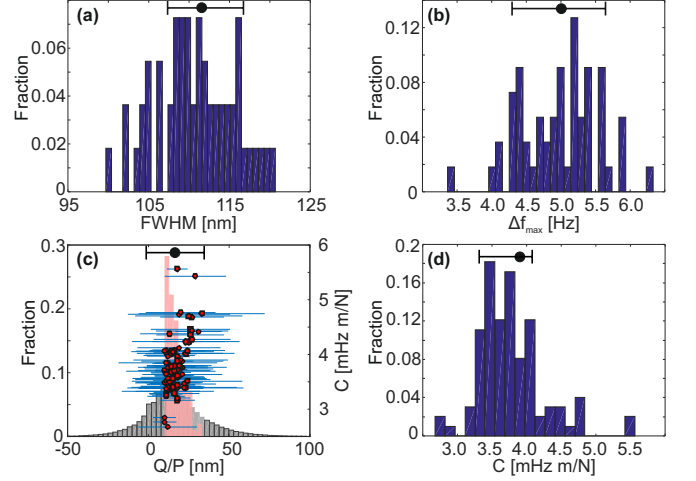


FIG. 4. (a,b) Histograms of the FWHM and Δf_{max} . (c) Histograms of Q/P and a plot of C vs. Q/P . The large error bars reflect the proximity of the resolution limit. The narrow distribution in (c) is directly from the fit, while the wide distribution is derived by accounting for the large error bars by assuming they are normally distributed. (d) Histogram of C . [The black bars with the large dot show the mean and a 70% confidence interval around it.]

by the error shown in the plot of C vs. Q/P in Fig. 4(c). Crucially, we can conclude that $\langle Q/P \rangle \simeq 17 \text{ nm}$ (standard deviation of 18 nm). Integrating the wide histogram we find that Q/P is positive with probability 0.82 . This likely rules out Bloch skyrmions ($Q = 0$) and implies that our skyrmions have Néel texture with helicity $|\gamma| < \pi/2$. While this is consistent with Néel skyrmions with helicity $\gamma = 0$ [Fig. 2(a)], we cannot rule out the presence of a partial Bloch component [40].

Figure 4(d) shows that the spread in C is relatively small compared to Q/P . Figure 4(c), which gives the spread in Q/P and C , shows no correlation between these two fit parameters. The contrasting spreads of Q/P and C are likely due to the inherent sensitivity of the latter to P , rather than to Q/P . Q/P provides finer information on the skyrmion structure [30], and is therefore more sensitive to disorder, which would in turn contribute its spread.

In summary, we have shown that MFM images of skyrmions can be quantitatively reproduced by modeling the magnetic field from a skyrmion using a closed expression from a multipole expansion, with several insightful conclusions. First, based on $|Q/P| \gtrsim 0$ we can rule out with $\approx 80\%$ certainty the skyrmions in Ir/Fe/Co/Pt multilayers as purely Bloch textured. Second, the sign of Q/P independently establishes the qualitative identification of the skyrmions in Ir/Fe/Co/Pt multilayers as possessing Néel texture with helicity $|\gamma| < \pi/2$, consistent with theoretical calculations [41]. Third, the magnitude of Q/P gives an estimate for d_{Sk} : $0 \lesssim d_{\text{Sk}} \lesssim 40 \text{ nm}$ for $\gamma = 0$. Fourth, the quantitative spread of d_{Sk} and the amplitude can be directly used to estimate the cor-

responding inhomogeneity of magnetic interactions. In particular, Δf_{\max} [shown in Fig. 4(b)] is expected to be sensitive to variations in D [29]. Finally, the utility of the physical analysis we presented beyond MFM, the compatibility with device configurations, and the relative computational simplicity that allows to apply it easily to large arrays of skyrmions, all bode well for real-world applications.

We are grateful for input from D. Arovas, K. Kuchuk, D. Podolsky, Y. Shechner, I. Schlesinger, U. Sivan, and A. Turner. The work in Technion was supported by the Israel Science Foundation (Grant no. 1897/14). The work in Singapore was supported by the Ministry of Education (MoE) – Academic Research Fund (Ref. No. MOE2014-T2-1-050), the National Research Foundation – NRF Investigatorship (Reference No. NRF-NRFI2015-04), and the A*STAR Pharos Fund (1527400026). We would also like to thank the Micro Nano Fabrication Unit at the Technion.

* christos@ntu.edu.sg

† ophir@physics.technion.ac.il

- [1] N. Romming, C. Hanneken, M. Menzel, J. E. Bickel, B. Wolter, K. von Bergmann, A. Kubetzka, and R. Wiesendanger, *Science* **341**, 636 (2013).
- [2] C. Moreau-Luchaire, C. Moutafis, N. Reyren, J. Sampaio, C. A. F. Vaz, N. Van Horne, K. Bouzehouane, K. Garcia, C. Deranlot, P. Warnicke, P. Wohlhüter, J.-M. George, M. Weigand, J. Raabe, V. Cros, and A. Fert, *Nat. Nano.* **11**, 444 (2016).
- [3] S. Woo, K. Litzius, B. Krüger, M.-Y. Im, L. Caretta, K. Richter, M. Mann, A. Krone, R. M. Reeve, M. Weigand, P. Agrawal, I. Lemesch, M.-A. Mawass, P. Fischer, M. Kläui, and G. S. D. Beach, *Nat. Mater.* **15**, 501 (2016).
- [4] O. Boulle, J. Vogel, H. Yang, S. Pizzini, D. de Souza Chaves, A. Locatelli, T. O. Mentes, A. Sala, L. D. Buda-Prejbeanu, O. Klein, M. Belmeguenai, Y. Roussigné, A. Stashkevich, S. M. Chérif, L. Aballe, M. Foerster, M. Chshiev, S. Auffret, I. M. Miron, and G. Gaudin, *Nat. Nano.* **11**, 449 (2016).
- [5] N. Nagaosa and Y. Tokura, *Nat. Nano.* **8**, 899 (2013).
- [6] A. Soumyanarayanan, N. Reyren, A. Fert, and C. Panagopoulos, *Nature* **539**, 509 (2016).
- [7] R. Wiesendanger, *Nature Reviews Materials* **1**, 16044 (2016).
- [8] G. Finocchio, F. Büttner, R. Tomasello, M. Carpentieri, and M. Kläui, *J. Phys. D: Appl. Phys.* **49**, 423001 (2016).
- [9] W. Kang, Y. Huang, X. Zhang, Y. Zhou, and W. Zhao, *Proc. IEEE* **104**, 2040 (2016).
- [10] N. Romming, A. Kubetzka, C. Hanneken, K. von Bergmann, and R. Wiesendanger, *Phys. Rev. Lett.* **114**, 177203 (2015).
- [11] W. Jiang, P. Upadhyaya, W. Zhang, G. Yu, M. B. Jungfleisch, F. Y. Fradin, J. E. Pearson, Y. Tserkovnyak, K. L. Wang, O. Heinonen, S. G. E. te Velthuis, and A. Hoffmann, *Science* **349**, 283 (2015).
- [12] X.-Z. Yu, Y. Onose, N. Kanazawa, J. H. Park, J. H. Han, Y. Matsui, N. Nagaosa, and Y. Tokura, *Nature* **465**, 901 (2010).
- [13] S. Mühlbauer, B. Binz, F. Jonietz, C. Pfleiderer, A. Rosch, A. Neubauer, R. Georgii, and P. Böni, *Science* **323**, 915 (2009).
- [14] M. Lee, W. Kang, Y. Onose, Y. Tokura, and N. P. Ong, *Phys. Rev. Lett.* **102**, 186601 (2009).
- [15] N. S. Kiselev, A. N. Bogdanov, R. Schäfer, and U. K. Rößler, *J. Phys. D: Appl. Phys.* **44**, 392001 (2011).
- [16] P. Milde, D. Köhler, J. Seidel, L. M. Eng, A. Bauer, A. Chacon, J. Kindervater, S. Mühlbauer, C. Pfleiderer, S. Buhrandt, C. Schütte, and A. Rosch, *Science* **340**, 1076 (2013).
- [17] A. Fert, *Materials Science Forum* **59-60**, 439 (1990).
- [18] M. Bode, M. Heide, K. von Bergmann, P. Ferriani, S. Heinze, G. Bihlmayer, A. Kubetzka, O. Pietzsch, S. Blügel, and R. Wiesendanger, *Nature* **447**, 190 (2007).
- [19] A. K. Nandy, N. S. Kiselev, and S. Blügel, *Phys. Rev. Lett.* **116**, 177202 (2016).
- [20] A. Soumyanarayanan, M. Raju, A. L. G. Oyarce, A. K. C. Tan, M.-Y. Im, A. P. Petrovic, P. Ho, K. H. Khoo, M. Tran, C. K. Gan, F. Ernult, and C. Panagopoulos, *arXiv:1606.06034* (2016).
- [21] F. Büttner, C. Moutafis, M. Schneider, B. Krüger, C. M. Günther, J. Geilhufe, C. von Korff Schmising, J. Mohanty, B. Pfau, S. Schaffert, A. Bisig, M. Foerster, T. Schulz, C. A. F. Vaz, J. H. Franken, H. J. M. Swagten, M. Kläui, and S. Eisebitt, *Nat. Phys.* **11**, 225 (2015).
- [22] W. Legrand, D. Maccariello, N. Reyren, K. Garcia, C. Moutafis, C. Moreau-Luchaire, S. Collin, K. Bouzehouane, V. Cros, and A. Fert, *Nano Lett.* **17**, 2703 (2017).
- [23] S. Heinze, K. von Bergmann, M. Menzel, J. Brede, A. Kubetzka, R. Wiesendanger, G. Bihlmayer, and S. Blügel, *Nat. Phys.* **7**, 713 (2011).
- [24] J. F. Pulecio, A. Hrabec, K. Zeissler, R. M. White, Y. Zhu, and C. H. Marrows, *arXiv:1611.06869* (2016).
- [25] Y. Dovzhenko, F. Casola, S. Schlotter, T. X. Zhou, F. Büttner, R. L. Walsworth, G. S. D. Beach, and A. Yacoby, *arXiv:1611.00673* (2016).
- [26] V. Cros, R. Wiesendanger, C. Marrows, R. Stamps, S. Blügel, S. Heinze, J. Raabe, and C. Moutafis, *arXiv:1609.08415* (2016).
- [27] A. Hrabec, J. Sampaio, M. Belmeguenai, I. Gross, R. Weil, S. M. Chérif, A. Stachkevitch, V. Jacques, A. Thiaville, and S. Rohart, *arXiv:1611.00647* (2016).
- [28] S. Husain, N. Sisodia, A. K. Chaurasiya, A. Kumar, S. Akanse, A. Barman, P. K. Mudulli, P. Svedlindh, and S. Chaudhary, *arXiv:1703.10224* (2017).
- [29] M. Baćani, M. A. Marioni, J. Schwenk, and H. J. Hug, *arXiv:1609.01615* (2016).
- [30] See Supplemental Material.
- [31] T. R. Albrecht, P. Grütter, D. Horne, and D. Rugar, *J. Appl. Phys.* **69**, 668 (1991).
- [32] F. J. Giessibl, *Phys. Rev. B* **56**, 16010 (1997).
- [33] A. O. Leonov, T. L. Monchesky, N. Romming, A. Kubetzka, A. N. Bogdanov, and R. Wiesendanger, *New J. Phys.* **18**, 065003 (2016).
- [34] Typical magnetic parameters for our sample are $A = 12$ pJ/m, $D = 2.5$ mJ/m², $K = 0.20$ MJ/m³, $\mu_0 H = 0.38$ T and $M_s = 1.02$ MA/m. In this case $L_D = 60$ nm, $K_0 = 0.13$ MJ/m³, $B_D = 0.26$ T and consequently $k = 1.54$ and $b = 1.47$.
- [35] J. D. Jackson, *Classical Electrodynamics*, 3rd ed. (Wiley,

- New York, 1998).
- [36] L. Luan, O. M. Auslaender, T. M. Lippman, C. W. Hicks, B. Kalisky, J.-H. Chu, J. G. Analytis, I. R. Fisher, J. R. Kirtley, and K. A. Moler, *Phys. Rev. B* **81**, 100501 (2010).
 - [37] Y. Lamhot, A. Yagil, N. Shapira, S. Kasahara, T. Watashige, T. Shibauchi, Y. Matsuda, and O. M. Auslaender, *Phys. Rev. B* **91**, 060504 (2015).
 - [38] A. Moser, H. J. Hug, B. Stiefel, and H.-J. Güntherodt, *J. Magn. Magn. Mater.* **190**, 114 (1998).
 - [39] E. W. J. Straver, J. E. Hoffman, O. M. Auslaender, D. Rugar, and K. A. Moler, *Appl. Phys. Lett.* **93**, 172514 (2008).
 - [40] J. Rowland, S. Banerjee, and M. Randeria, *Phys. Rev. B* **93**, 020404 (2016).
 - [41] H. Yang, O. Boulle, V. Cros, A. Fert, and M. Chshiev, *arXiv:1603.01847* (2016).
 - [42] H. Yang, A. Thiaville, S. Rohart, A. Fert, and M. Chshiev, *Phys. Rev. Lett.* **115**, 267210 (2015).
 - [43] J. Cho, N.-H. Kim, S. Lee, J.-S. Kim, R. Lavrijsen, A. Solignac, Y. Yin, D.-S. Han, N. J. J. van Hoof, H. J. M. Swagten, B. Koopmans, and C.-Y. You, *Nat. Commun.* **6**, 7635 (2015).